JAERI-Research
99-069

ON THE DEVELOPMENT OF LWR FUEL ANALYSIS CODE (1)
— ANALYSIS OF THE FEMAXI CODE AND PROPOSAL OF A NEW MODEL —

January 2000

Sergei LEMEHOV and Motoe SUZUKI

日本原子力研究所
Japan Atomic Energy Research Institute

本レポートは，日本原子力研究所が不定期に公刊している研究報告書です。
入手の問合わせは，日本原子力研究所研究情報部研究情報課（〒319-1195　茨城県那珂郡東海村）あて，お申し越しください。なお，このほかに財団法人原子力弘済会資料センター（〒319-1195　茨城県那珂郡東海村日本原子力研究所内）で複写による実費頒布をおこなっております。

This report is issued irregularly.
Inquiries about availability of the reports should be addressed to Research Information Division, Department of Intellectual Resources, Japan Atomic Energy Research Institute, Tokai-mura, Naka-gun, Ibaraki-ken, 319-1195, Japan.

編集兼発行　　日本原子力研究所

JAERI-Research 99-069

On the Development of LWR Fuel Analysis Code (1)
- Analysis of the FEMAXI code and Proposal of a New Model -

Sergei LEMEHOV and Motoe SUZUKI

Department of Reactor Safety Research
Nuclear Safety Research Center
Tokai Research Establishment
Japan Atomic Energy Research Institute
Tokai-mura, Naka-gun, Ibaraki-ken

(Received November 29, 1999)

This report summarizes the review on the modeling features of FEMAXI code and proposal of a new theoretical equation model of clad creep on the basis of irradiation-induced microstructure change.

It was pointed out that plutonium build-up in fuel matrix and non-uniform radial power profile at high burn-up affect significantly fuel behavior through the interconnected effects with such phenomena as clad irradiation-induced creep, fission gas release, fuel thermal conductivity degradation, rim porous band formation and associated fuel swelling. Therefore, these combined effects should be properly incorporated into the models of the FEMAXI code so that the code can carry out numerical analysis at the level of accuracy and elaboration that modern experimental data obtained in test reactors have.

Also, the proposed new mechanistic clad creep model has a general formalism which allows the model to be flexibly applied for clad behavior analysis under normal operation conditions and power transients as well for Zr-based clad materials by the use of established out-of-pile mechanical properties. The model has been tested against experimental data, while further verification is needed with specific emphasis on power ramps and transients.

Keywords: LWR, Fuel, Burnup, Plutonium Build-up, Clad Creep, FEMAXI Code

軽水炉燃料解析コードの開発について（１）
—FEMAXIの分析と新モデルの提案—

日本原子力研究所東海研究所安全性試験研究センター原子炉安全工学部

Sergei LEMEHOV・鈴木　元衛

（1999年11月29日　受理）

本報告は、FEMAXI-Vコードモデルの特徴のレビュー、及び、被覆管クリープの、照射誘起微細組織変化に基づく新しい理論的モデル式の提案をまとめたものである。

高燃焼度におけるマトリックスへのPu蓄積及び半径方向出力プロファイルの不均一性は、被覆管の照射誘起クリープ、FPガス放出、燃料熱伝導率低下、リム層ポーラスバンド形成、それと関連したスエリングなどの現象と相互に連関することにより燃料ふるまいに大きく影響することを指摘した。したがって、これらの連関効果はFEMAXI-Vコードのモデルに正しく組み入れられるべきであり、それによりコードは、試験炉で得られる実験データの持つ正確さと詳細さに匹敵するレベルの数値解析が可能となる。

また、被覆管のクリープに関して提案した新モデルは一般的な形に定式化されているので、炉外試験で得られた機械的性質を用いて、定常状態及び過渡変化時のZrベースの被覆管のふるまいの解析に柔軟に適用可能となる。本モデルは、実験データにより評価されたが、なお特に出力変動時及び過渡時について検証が必要である。

東海研究所：〒319-1195　茨城県那珂郡東海村白方白根2-4

CONTENTS

目　　次

1. INTRODUCTION

The temperature distribution in LWR fuels controls most of the physical processes having taken place during irradiation. With burnup increase thermal properties of fuel rods become more and more important since burnup-induced effects and enhancement of kinetic processes such as fission gas release, thermal conductivity degradation, micro restructuring and formation of high burnup UO_2 structure in the rim region of fuel. Proper understanding and adequate prediction of fuel thermal response are of prime importance for evaluation of fuel rod performance under base load irradiation conditions and transients.

The computer codes such as FEMAXI, FRAPCON and TRANSURANUS (most advanced among many others) are complex tools where many models for individual processes are incorporated and integrated in one body. The thermomechanical models in these codes have been extensively benchmarked. The database was established through measurements in research reactors and post irradiation examinations of tested and full scale commercial fuel rods. This is extremely important to validate thermal behaviuor of fuel rods. But the nature of burnup or fluence induced effects both in cladding and fuel matrix is still not so clear and need more analytical (mechanistic) models applicable for transients, post-transients and steady state conditions.

It is important to notice that the higher fuel burnup in commercial LWR reactors the higher role of theoretical models because of the flexibility that they can provide. The main issue is verification and validation of them, but that is the next step, which should be made. Empirical and semi-empirical models rely on experimental data and their flexibility in term of applicability for scientific analysis of fuel rod performance is easily questionable beyond the validated range. This is inherent limitation.

The point is that high burnup phenomena are known mainly due to post irradiation tests and only a few in-pile measurements of central temperature and integral fission gas release are available from Halden HBWR reactor, French, German and Japanese research facilities where conditions differ considerably from actual conditions at commercial reactors. Furthermore, integral parameters can only confirm importance of high burnup-induced phenomena but do not investigate them. Again, theoretical modelling establishes reasonable bridge between experiments and practical applications that should be made based upon them.

Commercial LWR fuel rods late in reactor life experience gap closing and pellet-clad interaction becomes one of the dominant factors leading to coupling thermal and mechanical analysis. Irradiation influences the rate of clad creep down, gap close and response on changes in operation conditions. The special focus for modelling is on accumulating of defects and micro-structural changes in polycrystalline clad materials influencing creep rate and radiation growth.

An accurate calculation of fuel and cladding deformation is necessary in any fuel rod response analysis because the heat transfer coefficient across the fuel-cladding gap is a function of both the effective fuel-cladding gap size and the fuel-cladding interfacial pressure. In addition, an accurate calculation of stresses in the cladding is needed to accurately calculate the onset of cladding failure (and subsequent release of fission products). Practically important question is how much relaxation cladding can have after long base irradiation or being subjected to RAMP transients. That is why theoretical modeling of creep phenomena is needed. However, complexity of such model should be properly adjusted to complexity of fuel performance code being used for thermomechanical analysis, in this particular case for FEMAXI code.

One specific effect plays a special role both in thermal and mechanical response analysis. This is formation of high burnup UO_2 structure accomplished with development of porous (spongy like) band in the rim region due to extremely high local burnup caused by plutonium buildup. Generally, the burnup at the rim is about twice as high as the average cross-sectional value. Porous band looks like a multiphase system containing very fine sub-micron UO_2 particles and a population of faceted gas pores. The width of the porous band apparently increased with burnup and it is around 50 μm wide at ≈ 45 MWd/kgU and more than 120-150 μm wide at cross-sectional burnup > 55 MWd/kgU.

Naturally, the porous band at high fuel burnup plays a role of additional thermal barrier due to highly degraded local thermal conductivity and increase in percentage of gas porosity. The latter is 10 to 50 % of theoretical UO_2 density. However, under normal steady state irradiation conditions in a commercial power reactor the rim porous band does not seem contribute greatly to integral fission gas release with burnup increase because the linear heat rate and fuel temperature decrease with each successive reactor cycle.

Nevertheless, reactor-history dependence of specific high burnup UO_2 structure development at the fuel surface can cause the onset of hard pellet-clad interaction when the rate of contra (relaxation) process in fuel and cladding are low due to temperature and hardening effect correspondingly.

At power transients situation might be even more dramatic. The higher accumulated cross-sectional burnup the higher fuel temperature and integral fission gas release. This is mainly because of the deterioration in the fuel thermal conductivity with burnup in volume and in the rim, particularly, the porous band which is very effective thermal barrier and additional powerful source of fission gas release to free volume.

The process by which the porous band at the UO_2 surface forms has not been yet established beyond doubt and there is strong necessity in developing mechanistic model for that. It appears certain due to a number of investigations [1-5] that it is a consequence of the high local burnup and fission gas concentrations, which are due to a buildup of fissile plutonium isotopes ^{239}Pu and ^{241}Pu.

This report describes a new original model, which is clad creep model, following analysis of the FEMAXI code models of special interest in a context of LWR fuel rod behaviour at high burnup.

2. ANALYSIS OF THE FEMAXI CODE

The principal tools of one of the prime importance in Fuel Safety Research Laboratory of JAERI are FEMAXI-IV and FEMAXI-V codes [6,7].

Several models are of special importance for accurate prediction of LWR fuel behaviuor at high burnup. These are

1. Fission gas generation, distribution through intra-granular and inter-granular gas bubbles and release to free fuel rod volume
2. Fuel thermal conductivity degradation in conjunction with formation of high burnup UO_2 microstructure
3. Radial power and temperature profiles, fission products and plutonium buildup distributions
4. Rim porous band formation and relationship between its properties and fuel rod thermal-mechanical response at high burnup
5. Fuel swelling due to high burnup and temperature induced formation of structural zones with specific properties across UO_2 fuel radius
6. Fuel pellet cracking, fragmentation and relocation
7. Cladding creep and related properties
8. Fuel side oxidation of cladding with burnup
9. Hot pressing and creep of UO_2 fuel under external PCI induced stresses at high burnup
10. Fuel-to-clad gap conductance

The review of these phenomena in relation with FEMAXI code is given bellow.

2.1 Fission Gas Release

In FEMAXI code, an equivalent sphere model is adopted to simulate the fission gas release [7]. The model allows prediction of beyond the range of experimental data, which cannot be supported by an empirical modeling. Fission gas release model is mechanistic model by status and considers two-stage release mechanism, that is diffusion of gas atoms to grain boundaries and saturation of grain boundaries accomplished by formation of inter-granular channels (bubbles) connected to fuel rod free volume. Additional fission gas release is assumed due to sweeping of gas atoms to grain boundaries by grain growth if temperature is high enough to support the process. Irradiation-induced resolution of gas atoms from tunnels (inter-granular bubbles) provides balance of gas atom concentration remaining if grain volume. The volume diffusion is considered accompanied by trapping of diffusing gas atoms at intra-granular gas bubbles. The partial amounts of gas atoms trapped at the bubbles and in a lattice are controlled by trapping and re-solution probabilities, which are calculated model parameters. The code prediction for benchmark cases [8] gives very satisfactory results for calculated fission gas release against qualified experimental data [9]. However, some modifications might improve flexibility of the fission gas model in FEMAXI code.

Consideration of intragranular bubble formation seems too simplified. For instance, the number of bubbles generated per each fission fragment is assumed constant, i.e. 24 bubbles per fission fragment. Meanwhile, there are strong experimental evidences that the density of intragranular bubbles is a function of fission rate, temperature and concentration of fission gas atoms in grain volume [9-12]. Furthermore, under irradiation up to high burnup the development of intragranular bubbles is bimodal. In addition to bubbles with high volume density and small sizes, which are 10^{17}-10^{18} per cm^3 by order and 1 to 6 nm in diameter correspondingly, the intragranular bubbles with low volume density ($10^{15}/cm^3$) and large sizes (10 to 200 nm) are formed [2]. Low-density population is able to accumulate a considerable amount of fission gas atoms generated in volume and virtually reduce concentration of lattice gas and local fission gas release to tunnels and free volume. This is essential for thermal response analysis during power transients late in fuel life.

Another modification that might be necessary is related to probability of resolution (re-dissolution) of gas atoms into the matrix from intragranular bubbles caused by interaction with passing high energetic fission fragments. In presently used model this probability is postulated to be proportional to square average size of intragranular bubbles. The point is that regular (small) intragranular bubbles hardly can survive in a collision with fission

fragment creating local distraction (displacement spike) of approximately 6 μm long and 10 nm in a diameter. A single fission fragment colliding with, or passing close to them, may destroy completely the bubbles. Because of this, the life of intragranular bubbles is limited and depends on fission rate density and volume covered by two fission fragments. In other words the resolution probability in volume is dynamic factor, which is rather independent (!) of size of intragranular bubbles. The available experimental evidences [13, 14] favor such interpretation [15] of the re-solution process, and have indicated [13] that instantaneous bubble destruction is most likely possible for bubbles up to 14 to 34 nm diameter. This correction should redefine balance between gas atoms in lattice and bubbles.

Next two remarks are more general.

The FEMAXI code has adopted the diffusion coefficient derived by J. Turnbull et al. [16] based on analysis of apparent fission gas release and irradiation enhancement has not presented in the obtained form. There are only two thermal terms and one athermal term.

However, even earlier research on growth of intragranular gas bubbles showed existence of so-called irradiation enhanced diffusion. The appearance of bubbles on straight lines following irradiation promotes the view that bubble nucleation occurs in the vicinity of displacement spikes, which leave a vacancy reach region in their wake. These lines of bubbles decorating fission tracks at temperatures 750 to 1800 ^{0}C have been observed under conditions where most of the gas is believed to be in solution and it is high concentration of vacancies in tracks that enhance the nucleation of bubbles. White at el. showed [17] that diffusion of fission products is enhanced below ~ 1400 ^{0}C and introduced three term diffusion coefficient, i.e. athermal form proportional to fission rate, irradiation-enhanced and thermally activated Arrhenius forms.

The second term depends on the square root of fission rate density as well as temperature with very low activation energy. Theoretical explanations of three-term irradiation induced and enhanced diffusion coefficient have been given in ref. [18].

Incorporating three-term diffusion coefficient into FEMAXI fission gas release model should properly adjust it to observed experimental data and correct calculation of balance between gas in solution (lattice gas) and intragranular bubbles and hence make more adequate prediction of gas swelling. It is important to note that corrections discussed need no significant modifications of the basic two-step mechanism of fission gas release implemented in the FEMAXI code.

Grain boundary resolution of fission gas atoms populating intergranular bubbles or tunnels play extremely significant role in controlling not only incubation threshold for fission gas release, but also the concentrations of gas atoms in grain volume and in resolution affected layer near grain boundaries. It is grains boundary resolution that prevents unlimited fission gas release to free volume after development of linkage between bubbles faceted the grain or/and grain edge tunnels.

It is postulated in the fission gas release model of FEMAXI code that the width or thickness of resolution layer on grain boundaries is a constant chosen to be equal 20 nm. In fact, that is a dynamic parameter, which can be derived from the first principles in terms of irradiation-induced and enhanced diffusion enabled by fission fragments passing the intergranular gas pores. The number of fission fragments passing through intergranular gaseous pore as well as number of gas atoms influenced by spikes on the pore surface are calculated parameters depending on fission rate density, partial gas pressure and gaseous composition in the pore. If athermal, irradiation-enhanced and thermal partial diffusion coefficients are known, the width of resolution layer is simply $\delta_r \propto \sqrt{(D_{ath} + D_{enh} + D_{Arh}) \times t_f}$, where $t_f = b_f^{-1}$ is the lifetime of a displacement spike. This width is controlled by instantaneous generation of new fission spikes, that is, $b_f = \frac{\pi}{2} \dot{F} \times \lambda_f \times d_f^2$ where $\dot{F}, \lambda_f, d_f^2$ are the actual fission rate density, range and characteristic diameter of the displacement spike, respectively.

In other words, the grain boundary resolution width is a constant of material only at very low temperatures where athermal diffusion takes place. The higher fuel temperature or low fission rates density the deeper width of resolution layer. The concentration of gas atoms in the resolution layer should be determined from balance of incoming and outcoming gas atoms. In fact, resolution effect creates a concentration barrier that prevents instantaneous gas release from grain volume under both steady-state operation and transients. The higher gas pressure in tunnels or intergranular gas bubbles faceted grains the higher concentration barrier. The temperature dependence is reverse. Due to dynamic character of concentration barrier in resolution controlled layer, reduction of heat generation rate will result in decreasing of this concentration barrier and also occur additional very fast release of excess gas from resolution layer and vicinity to grain porosity and free volume.

This is considered to be important modification for FEMAXI code fission gas release model and might improve predictability of the code in thermal response analysis.

2.2 Fuel Thermal Conductivity as a Function of Burnup

The initial thermal conductivity correlations are well established for all oxide fuels used in commercial reactors. The influences of parameters such as temperature, stochiometry, plutonium content and gadolinium content are relatively well known [19]. It is long shown that irradiation damage and the progressive buildup of plutonium and fission products with increasing fuel burnup in UO_2 and MOX fuels should correlatively reduce their thermal conductivity. The low the temperature, the stronger the effect predominantly controlled by phonon-phonon form of heat transfer. The burnup effect on thermal conductivity has been assessed up to 80 MWd/kgU by means of in-pile centerline temperature measurements and out-of-pile thermal diffusivity measurements with reasonable agreement between these two methods. However, the rim thermal conductivity evolution is not yet clearly known. The thermal degradation due to the onset of numerous sub-micron gas pores and degree of balancing by the "cleaning" of the fuel matrix subsequent to this porosity development is not properly understood.

The FEMAXI code has a number of models for calculating the fuel thermal conductivity as a function of local burnup and temperature. Correlations are typically derived from benchmarked measurements of steady-state centerline fuel temperature from instrumented fuel rods at Halden HBWR reactor when increase in central temperature per unit increase in the local linear heat rate is recorded.

However these data are not definitive regarding dynamic factors during power transients and microstructure changes in outer fuel surface (rim region) or in the transient zone. This zone is the next one by moving on towards the fuel center, where gas porosity is increased and sub-grains within course grain structure are exist. Particularly interesting is the fact that transient-tested fuels exhibit a region where gas bubbles in the grains are highly inhomogeneously dispersed resulting decoration of sub-grains as well as grains and bubble denuded zones [1]. The fuel thermal conductivity degradation due to gas bubbles and high burnup UO_2 structure formation is unlikely the same as determined for a fresh porous fuel because the difference between helium and fission gas in term of thermal resistance is considerable.

Comparison of the EPMA and puncturing results supports a suggestion that in transient-tested UO_2 fuel rods a large percentage of gas release from the grains (locally 50-60 % depending on the burnup) are not able to reach the rods free volume and is retained on the grain boundaries or large bubbles. From the first principles, it is appear certain, that burnup-induced degradation of fuel thermal conductivity is a consequence of fission gases and buildup of volatiles with increasing burnup. The conductivity is a function of state of point defects, dislocation loops, and precipitates as well as gas bubbles (porosity) [19]. Logically, for transient response analysis the degradation should be re-formulated in terms of concentrations of fission products rather than as burnup dependent function. In other words, models of thermal conductivity and fission gas release have to become inextricably linked. There must be a model, which describes state and the balance between buildup, diffusion and irradiation-induced resolution for local conditions and hence, the fractions of fission products that exist as lattice gas and in gas bubbles.

Thus, such advanced model for thermal conductivity becomes intimately associated with other models of fission product release and their attendant complications.

Furthermore, the option for no crack factor reduction in the fuel thermal conductivity is supposed in the most of the fuel codes. This fact ignores not only radial cracks but circumferentially oriented micro- and macrocracks as well that should be treated as an additional porosity at least. Importance of crack factor reduction in effective thermal conductivity of UO_2 fuels has been demonstrated in calculating analysis of IFA-503.1 Halden test [20].

2.3 Radial Power and Temperature Distributions

In order to provide a reliable assessment of fuel thermal performance it is critical to calculate temperatures and their distribution as accurately as possible. Radial power distribution is a function of great importance in view of that goal.

The power and burnup radial distribution functions in FEMAXI code are input function-parameters generated by external neutronic code RODBUN [21]. The flexibility and integrity of the FEMAXI code can be virtually improved by incorporating an optional model or models in a manner as it was made in TRANSURANUS and FRAPCON-3 codes [5, 22]. In these codes a special shape function (form factor) governs the radially dependent buildup of the plutonium with effective cross-sections for uranium and plutonium isotopes of interest. The structure of FEMAXI code enables application of fine mesh placement near

fuel surface and coupling of power, plutonium buildup and burnup profiles with fission gas release model and models that have to calculate high burnup-induced effects in a fuel rod as well as temperature distribution in conjunction with them.

Similar approach has been already adopted and tested in ASFAD code [23] where original model for plutonium buildup and power rate distribution is used. Advanced modification of this model can be transferred to FEMAXI code. This new model is a symbiosis of the well-known TUBRNP model of Lassmann et al. [5] and RADAR model of Palmer et al. [24].

2.4 Rim Porous Band Formation

Rim porous band formation and high burnup UO_2 structure formation as a function of local burnup and temperature are the most important modification of FEMXI code that might be made because of specific importance for transient thermal response analysis. Experimental observations showed [1] that the surface of the fuels irradiated as high as above 45 MWd/kgU at steady-state operation can be highly porous, that is, porosity is up to 30-50 %. Integral release of fission gas from the porous band was found to reach 25 % and considerably contribute to total fission gas release to free fuel rod volume. Thus, it is very important to have a mechanistic model to calculate porous band formation in conjunction with local fission gas release.

The mechanism by which the porous band at the UO_2 surface forms is not established yet beyond doubt. However, it appears certain, that this is a consequence of the high local concentration of fission gases due to buildup and fission of plutonium. Two models, that is, semi-empirical and mechanistic respectively, have been already published in open literature on this concern [4, 25]. The complexities of the models enable application both of them in the FEMAXI code.

2.5 Fuel Swelling

Fuel swelling due to high burnup and temperature induced formation of structural zones with specific properties across UO_2 fuel radius is virtually related to previous discussion. Highly irradiated fuel has a specific zone structure controlled by temperature, burnup, and irradiation history. These zones are classified as follows [1,2]:

Zone 1. This is a fuel rim where the porous band has occurred with percentage of gas porosity up to 30-50 % in fully developed high burnup structure.

Zone 2. This zone is the next one, situated in the cold outer part of the fuel matrix and consists of coarse grains and sub-grains with enlarged intragranular porosity and intergranular initial pores that undergone some irradiation-induced sintering.

Zone 3. This zone is detected when only intergranular bubbles decorating grains are presented.

Zone 4. This zone is designated when both intergranular and intragranular bubbles are present.

Zone 5. This zone is designated when fuel exhibits a region in which fuel grains are chequered by clusters of gas bubbles and bubble free areas showing effect of cleaning grains from lattice gas.

Zone 6. This is a typical high temperature zone with dramatic variation in bubble density, grain edge tunnels and/or grain growth and columnar re-crystallization.

Zone 7. This zone is designated when columnar grain formation has occurred.

An advance model is needed, which could describe micro and macro restructuring, porosity evolution and gas bubble formation, which are being intimately associated with models of fission gas release, redistribution of lattice gas along different secondary states (bubbles, dislocation loops, tunnels) and all their attendant complications.

There is every reason to suppose that these zones will have an impact on transient and steady state thermal behaviour of LWR fuel rods. Implementation of zone model in context of swelling is appreciable for coupling of thermal and mechanical analysis.

2.6 Fuel Pellet Cracking, Fragmentation and Relocation

The close coupling of the thermal and mechanical modelling is the consequence of the existence of the fuel-to-clad gap. As the temperature increases, the stresses resulting from temperature gradient in the fuel matrix causes the fuel crack, fragmentation and relocation. Cracks are formed both in the radial and circumferential directions. Void space, which is originally in the fuel-clad gap, is relocated into the fuel matrix as the fragments of fuel move outwardly into the gap. As the fuel becomes hotter, the fuel expands, filling some of the voids within the fuel. However, asperities do not align exactly, thereby causing the fuel diameter to appear larger and the fuel to interact with the cladding at a lower power than that

expected due to normal expansion (or contraction) mechanisms, including thermal expansion, swelling, and densification.

The cracks allows nearly 50% [22] of the original fuel surface relocation to be recovered due to fuel swelling before hard contact is established between the fuel and the cladding. The modeling of the cracked and relocated fuel, both thermally and mechanically, requires accounting for changed fuel-cladding gap size (and hence gap conductance) and the changed fuel pellet diameter as the fuel interacts with the cladding. The fuel surface relocation provides a new fuel-cladding gap size for calculating gap conductance and mechanical interactions. Also considered is the shift of voids from the fuel-cladding gap into the fuel pellet (and the resultant pressure change) and the feedback into the mechanics and thermal calculations.

To cope with cracks and relocation FEMAXI code has adopted a quite simple and sufficient model. However, two modifications would be made.

The data obtained in the IFA-503.1 WWER/PWR comparative Halden test [26] disclosed one very general principal result. At reference power levels the temperatures in the WWER and the PWR reference fuel rods differ no more than 25 ^{0}C.

Regardless of rather different densification behaviour the measured temperatures in WWER and PWR rods showed no principal deviations and were even slightly higher (within the 25 ^{0}C band) in PWR-reference rods. An explanation of this result has been analyzed [20, 27] and favored conclusions are as follows.

Early in life, the ceramic UO_2 fuel pellets crack, radially and axially, into numerous wedge-shaped fragments. Considerable roughness is associated with the surfaces of fragments. This roughness leads to a radial relocation of some gap volume to fuel due to crack propagation during reactor power changes, at start-ups and shutdowns. Generally, relocation depends on the number of radial cracks and degree of freedom associated with fuel fragments in a pattern. Due to in-pile densification the freedom mode of fuel fragments is increased. Densified fragments move relative to each other causing macroscopic relocation as a function of power rate and achieved bulk densification. This macroscopic relocation contributes to partial gap closure and to some "dynamic" degradation in effective (in-pile) fuel thermal conductivity because some cracks are circumferentially oriented. The radial relocation is permanently exists as combination of dynamic and kinetic functions.

The power dependence of partial gap closure due to relocation was found is to be proportional to the factor as follows:

$$F_{reloc} \propto Exp\left\{-\frac{q_L - q_{jump}}{q_{rel}}\right\},$$

where q_L is the linear heat generation rate, q_{jump} is some threshold corresponding to pellet jump effect, and q_{rel} is the dynamic parameter of relocation. M. Oguma [28] based on analysis of in-pile data for PWR and BWR fuels first introduced the pellet jump effect. It was suggested that pellet jump caused by cracking is a primary effect: no relocation takes place before that.

The pellet jump threshold can be calculated from the first principals, or alternatively, as best estimated model parameter chosen from in-pile data analysis. The contribution to fuel-to-clad gap closing corresponding to pellet jump is a constant effect being added to the permanent relocation resulting from relative mobility of the fragments.

The curvature, and in some cases a knee like deflection can be observed in the temperature versus linear heat rate correlation during the very first starts to power. Being interpreted in terms of rating dependence of the gap thermal conductivity temperature singularity favors an assessment for the pellet jump distance to pellet diameter ratio, C_{jump} that is close to $(3.6 \div 3.8) \times 10^{-3}$ for porous UO_2 sintered fuel pellets [29].

Very simple and efficient empirical correlation between initial microstructure of UO_2 fuel and threshold contribution to pellet-clad gap closure enables to assess the primary relocation (pellet jump). This is

$$C_{jump} \approx 6 \times \left(\frac{\Delta\rho}{\rho}\right)_{initial}$$

where $\left(\frac{\Delta\rho}{\rho}\right)_{initial}$ is the fraction of initial porosity associated with as-fabricated pores distributed in grain volume, double boundaries and grain corners [20].

M. Oguma has proposed another correlation for the pellet jump effect in a very pioneer work [28] in the form of prompt contribution, ΔD_{jump}, into an increase of pellet diameter, D_{fuel}, due to critical cracking:

$$\Delta D_{jump} = 3.6 D_{fuel} .$$

M. Oguma also proposed a semi-empirical correlation to calculate fuel-to-clad gap, which includes both dynamic and kinetic relocation effects in the form as follows:

$$G(bu, q_L) = \{1 - A \times f(bu)\} \times Exp\left\{-\frac{q_L - q_{jump}}{q_{rel}}\right\} \times \{G_0 - \Delta D_{jump} - \Delta G_t\}$$

Wherein

A is the numerical parameter;

$f(bu)$ is the function of pellet burnup, bu;

G_0 is the as-fabricated fuel-to-clad gap;

ΔG_t is the accumulative gap closure due to phenomena, which do not related with fuel cracking, e.g., swelling, thermal expansion, creep, etc.

Semi-theoretical modification of original correlation by M. Oguma has been presented in [20,27] in a similar form:

$$G(bu, q_L) = \left\{1 - \frac{1}{6C_{jump}}\left(\frac{\Delta\rho}{\rho}\right)_{densf}\right\} \times Exp\left\{-\frac{q_L - q_{jump}}{q_{rel}}\right\} \times \{G_0 - \Delta D_{jump} - \Delta G_t\}$$

where $\left(\frac{\Delta\rho}{\rho}\right)_{densf}$ is the net in-pile densification effect. This correlation is incorporated into the ASFAD code model library and has passed through a number of verification calculations against appropriate in-pile measurements of fuel centerline temperatures in test fuel rods with different gap sizes and filling gas compositions.

The major conclusion, which can be drown from discussion above is that in-pile densification of fuel fragments contributes to relocation and relocation itself is not additive sum of partial contributions from different particular phenomena, but rather complex nonlinear dynamic process. This phenomenon must be reviewed and properly modeled for code applications in view of great importance for steady state and transient thermal and mechanical analysis.

2.7 Cladding Creep and Related Properties

Mechanical analysis that enables FEMAXI code is the most advanced and sophisticated part of the code among many other fuel performance codes. Cladding creep due to misbalance between external and internal applied stresses is a part of mechanical calculations.

Cladding creep is important for modelling the size of fuel-to-clad gap and initial stored energy at the start of transients. In PWR fuel rods, the creep may be sufficiently rapid and affect fuel relocation and effective thermal conductivity of fuel pellets. FEMAXI code has adopted an empirical creep model, which is quite comprehensive for practical application for LWR fuel rods. However, the flexibility of model is limited. There is general remark that encourages development of new creep model.

More economic utilization of standard dioxide fuels demands going to higher fuel burnup without any loss of fuel rod reliability, flexibility margins and safety. Japan today is about to introduce fuel cycles with average discharged burnup in fuel assemblies as high as 55 MWd/kgU. This presumes that fuel assemblies have to be operated at higher linear heat rates and/or intervals between fuel reloading as well as in-reactor lifetime to be extended to 18 months or even longer and to four-five years, respectively. Also, Japan has long been committed to closing uranium fuel cycle by reprocessing spent fuel from LWR reactors to recover plutonium that would be recycled in mixed uranium-plutonium oxide (MOX) in LWR reactors and in fast breeder reactor as well. One can expect that Japan in near future will operate LWR reactors charged with MOX fuel assemblies along with standard UO_2 fuel. This all raises a number of issues to be resolved in a proper way and demands developing not only new technologies but new models as well. In particular, cladding materials that are currently used for fuel rods are to be advanced to face long irradiation and higher neutron fluence.

In LWR reactors high energy particles and fast neutrons are bombarding fuel rod cladding creating structure defects that result degradation of as-fabricated material properties. During the power transients in a later stage of in-reactor life, fuel failure and situations when fuel rod integrity may suffer will occur. That's why in Japan, as well as in the USA and worldwide new clad materials for LWR fuel rods are under development, testing and implementation.

For instance, in Japan there is very impressive and even ambitious development of a supper alloy having the world best high temperature strength and good formability with dual application both for fusion and fission reactors. It can be expected that safety and operability of Japanese LWR reactors will be more improved after industrial implementation of this supper alloy.

New cladding alloys are particular essential because there are solid evidences that uranium dioxide and MOX fuel have certain natural limitations in utilization that are about to be exceeded for part of fuel rods in assemblies with average discharge burnup of about 55 MWd/kgU. It is clearly understood now that after 40 to 50 MWd/kgU the properties of nuclear fuel are completely different from those of as-fabricated fuel. The role of cladding is greatly increased with progressing burnup. There must be a model, which describes the creep process with intimate association with models of irradiation-induced damages in clad materials and all attendant complications in order to cope with new clad materials and operation conditions in a flexible manner.

Many studies have been conducted in relation to the creep behaviour as one of the central parts of thermal and mechanical analysis with fuel performance code. Sets of different equations have been proposed. Still there are many uncertainties in understanding in understanding of the process since Nichols [30] to Mattews and Finnis [31]. Engineering models deal with restricted area of database applicability. Their flexibility in practice is limited: different operation conditions or post-reactor storage need rather different creep correlations. On the other hands, theoretical models become more and more theoretical and even academician and only increase the gap between practice and theory [31].

One of the first successful attempts in developing "flexible" creep model for LWR claddings has been made by N. E. Hoppe [32]. His model, semi-engineering by status, contains some important ideas that can be applied for further elaboration of mathematical description of creep phenomena with complexity admitted by practical application in fuel performance codes.

A new model has been proposed [33] and progressively developed is presented here in sections blow as an extension of Hoppe's model approach. The model entitled ***BNR***-creep model, i.e. **B**ingham-to-**N**ewtonian **R**elaxation of diffusion zones was constructed under ambitions "from first principals to principal applications".

The objective of this model is to predict creep properties of polycrystalline materials such as Zircalloy-4 in conjunction with main irradiation-induced effects that affect lattice microstructure. In details this model is described in a proper section of this report.

2.8 Fuel Side Oxidation of Cladding with Burnup

Fuel side oxidation of cladding or, in other words, formation of fuel-to-clad bonding layer is not currently taken in the FEMAXI code model analysis of fuel rod performance at high burnup. Meanwhile, modern studies of LWR fuels (e.g. [34,35]) disclose that at burnup of 40 MWd/kgU and higher the bonding layer 10 to 20 μm is formed by resulting unappreciable additional thermal resistance between fuel and clad. Also, it influences fuel and clad interference at high burnup and can make their contact harder at high burnup under steady state and transients.

The mechanisms responsible for formation of fuel-clad bonding layer are quite clear and have been indicated in details in the paper [35] and can be easily modeled.

2.9 Hot Pressing and Creep of UO_2 Fuel

One of the main objectives of computer code calculations is to demonstrate that margins of design flexibility and safety parameters are not exceeded with all respect to phenomena specifically attributed to high burnup induced changes in the fuel matrix and cladding. As it was discussed above, the in-reactor performance of LWR fuel rods at extended burnup is characterized by UO_2 restructuring and appearance of a number of structure zones containing gas porosity and secondary defects (i.e., irradiation-produced network dislocations, sub-grains). Gap closure in an active part of fuel rod will invoke pellet-clad mechanical interaction and stresses in fuel matrix, and as a result mechanical and chemical properties of cladding differ considerable from those of as fabricated. However, in despite of all these changes, LWR fuel rods still retain a considerable potential for relaxing contact stresses and for adjusting their behaviour to actual internal states and external conditions.

Hot-pressing (fuel creep accomplished with changes of volume) is one of the relaxation processes initiated by applied external stresses in result of hard contact between fuel and cladding. The rate of hot pressing is a function of parameters, which characterize irradiation condition (temperature, fission rate, and burnup), contact stresses and state of ceramic fuel, i.e. grain size, remaining porosity, and dislocation network. When the hard contact occurs in LWR fuel rod all structural zones will contribute to relaxation via local hot pressing which is differ for every specific zone.

Correlations, which are currently, used in fuel rod performance codes, are not able to cope with complexity of structural zones induced by burnup.

There must be a model, which describes creep behaviour and hot pressing of highly irradiated fuel respecting all structural complications.

2.10 Fuel-to-Clad Gap Conductance

The main thermal resistance in the LWR fuel rods is that of the fuel-to-clad gap as well as thermal conductivity of the pellet. Parameters that responsible for that are fuel to clad gap separation, surface roughness of fuel and cladding, gas composition in free volume, temperature of gas, gas pressure and eccentricity (the derivation between fuel axis and clad axis).

Traditionally, the gap conductance, h_{gap}, responsible for the temperature drop across the gap space is made up as the sum of three additive conduction routines, i.e. conductance through the gas gap, h_{gas}, conductance through areas of intimate contacts, h_{cont}, and radiative heat transfer, h_{rad}:

$$h_{gap} = h_{gas} + h_{cont} + h_{rad}$$

Until the onset of pellet-clad contact, the most important term with respect to the gap conductance is h_{gas} because its value depends critically on gas thermal conductivity and reversibly on the dimension of gap.

Despite the uncertainties in the gap size due to fuel pellet fragmentation and relocation, in-pile experiments verify the standard form of representation for conductance through the gas gap.

Thermal conductivity of xenon and helium is considerably different. Despite this fact, in fuel rods with very small gap sizes the difference between xenon and helium filled rods tends to vanishing [19]. This implies that effective heat conduction occurs through the solid-solid contact sports for which the filling gap gases play no important role. The gap conductance must therefor include a progressive flattering of asperity of fuel and clad separation with tightening of the gap size.

In order to model gap conductance it has been proved [19] necessary to modify additive sum of three terms $h_{gas}, h_{cont}, h_{rad}$ to a new form considering the stochastic nature of pellet fragmentation, dynamic relocation and eccentricity as well. Introducing a contact function F_{cont}, which should combine partial contributions from gas conduction and contact conduction, can enable this. One of the possible modifications is simple as that:

$$h_{gap} = (1 - F_{cont}) \times \bar{h}_{gas} + F_{cont} \times h_{cont} + h_{rad}$$

where F_{cont} is the fraction of pellet surface which are in intimate contact with cladding , and $\bar{h}_{gas}$ is the re-defined conductance through the gas gap in order to account averaged eccentricity effect that leads to the form as follows [36]:

$$\bar{h}_{gas} = \frac{h_{gas}}{\sqrt{1 - \left(\frac{\varepsilon \times \delta}{\delta + \xi + 2g} \right)^2}}$$

Wherein h_{gas} is the standard gas conductance through coaxial fuel-to-clad gas gap, ε is the averaged eccentricity between fuel pellets and clad, δ is the geometrical hot gap size, ξ is the combined roughness of the surfaces, and g is the "temperature jump distance" (accommodation effect) in the conventional form. This form has been obtained analytically by statistic averaging over random pellet distribution inside fuel rods. The suggestion implies that pellets in fuel rod are not exactly positioned along the center of the cladding, but rather eccentrically stationed being normally (randomly) distributed.

Function F_{cont} tends to the unit for the tightly closed gap, and zero for the large gap size. The simplest way is to derive such a function from experiment.

2.11 Conclusive summary

On the basis of the discussion above, it is concluded that modelling of all mentioned features continues to present a challenge from both a mathematical and physical points of view. But they must be properly addressed to face realities of high burnup. The great issue is to validate new models needed to improve adequacy of code calculations for high burnup fuel rods. Anyway, the first step (modifications) should be made in order to enable verification exercises.

3. A BNR MODEL FOR LWR FUEL ROD CLAD CREEP BEHAVIOUR

Semi-theoretical model was developed for predicting creep strain under thermal out-of-pile and in-pile conditions of interest for LWR type fuel rods. The results of model calculations were compared with an isothermal experiment data and post-irradiation examinations as available. Discussion was also given to the difference in creep behaviour between irradiated and unirradiated fuel cladding, indicating that model equations are applicable for predicting creep strain of spent fuel claddings. Strain-hardening and fluence/time-hardening effects were modeled and discussed.

3.1 Background

Clad creep behaviour of LWR nuclear fuel is one of the most important phenomena both for in-reactor fuel performance and post-reactor interim storage. Many studies have been conducted in relation to the creep behaviour of LWR fuel rod clad materials and a set of different creep equations have been proposed (see [40,41]). However, there are still many uncertainties in understanding of the process since F.A.Nichols [40] to J.R.Matthews and M.W.Finnis [41]. Engineering models deal with restricted areas of database applicability. Their flexibility is limited: different in-pile or lab tests or post-reactor storage need rather different models or correlations to be applied to fuel rod performance and integrity analysis. One of the first successful attempts in developing creep model for LWR claddings has been made by N.E.Hoppe [32]. His model – engineering by status – contains some important ideas that can be useful for further elaboration of mathematical description of creep phenomena. The present work was undertaken to suggest a new model approach to a uniform description of the LWR clad creep process with complexity admitted for applied fuel rod performance codes.

3.2 Radiation Damage Processes

Irradiation with fast neutrons enhances the self-diffusion coefficient and simply introducing such coefficients into the thermal diffusion creep equations leads to reasonable results at the temperatures of interest, i.e., below ~ $\frac{1}{2}T_m$. It is clear now owing to investigations by Nichols [30] and analysis by J.R.Matthews and M.W.Finnis [31].

The enhanced diffusion coefficient is supposed to arise from increased vacancy concentrations. The problem is that irradiation-enhanced diffusion models relay on the assumption that vacancy flow driven by long ranged gradients in the chemical potential of vacancies at different sites in the lattice microstructure. This assumption is required in order to include dislocation glide facilitated by climb or recovery. However, irradiation-enhanced concentrations of point defects play no role in vacancy thermal emission driven mechanisms and do not alter the concentration gradients between principal defect sinks. The dilemma has to be resolved in order to place confidence in irradiation enhanced diffusion creep modelling.

The point is that irradiation enhanced diffusion is just one of the consequences of the lattice micro-structural changes produced by fast neutrons and damage cascades created by them. C.C.Dollins [37] and W.J.Phythian [38] showed the importance of fast neutron irradiation-induced damaging on the temperature dependence of yield strength and radiation growth of Zircaloy.

For modelling, the radiation damage processes in polycrystalline materials will be considered first and quantitative treatment of damage cascades and their particular role will be proposed.

3.3 Primary Collisions and Damage Cascade

When a fast neutron collides with lattice atoms along its pathway these atoms receive a considerable portion of its energy (*the primary collisions*) enabling them to initiate a sequence of displacements in the lattice known as a damage cascade (*the secondary collisions*). At this stage thermodynamic as well as statistic equilibriums are broken.

3.4 Radiation Damage Quenching

Next, the cascade comes to thermal equilibrium and dominating recombination of vacancies and interstitial atoms in the damage cascade formed occurs, resulting in the

establishment of the initial size and coaxial double zone shape of the damaged region. It may be assumed that thermodynamic equilibrium has to be restored first resulting in minimization of excess internal free energy and then the system comes to statistic equilibrium between point defects (i.e., self-interstitial atoms and vacancies) and sinks such as voids, dislocations and grain boundaries. This assumption allows both equilibrium concentrations of point defects in cascade damage and the characteristic time scale of the quenching phase to become calculated values, and, thus, the partial radiation induced self-diffusion coefficient can be evaluated as well.

3.5 Radiation Damage Annealing

Some fraction of vacancies and interstitial atoms avoids recombination because of the stochastic nature of the process. The remaining point defects then diffuse thermally or recombine or can be captured by different sinks distributed inside the polycrystalline lattice. Sheared distribution of point defects in the formed damage cascade results by way of enhanced self-diffusion of point defects in that volume. It lasts until damage being annealed thermally and/or high-energy neutron collisions initiate a new generation of damage cascades.

3.6 Partial Self-Diffusion Coefficients

A three-stage approach to damage cascade formation and evolution provides quantitative assessments for three partial self-diffusion coefficients each associated with one of these stages. These partial coefficients according to their nature may be called irradiation-controlled, irradiation-enhanced and irradiation-induced partial self-diffusion coefficients, according to their nature.

The athermal irradiation-controlled coefficient, D_F, can be simply defined via the rate of generation of damage cascades, b_f, time scale, τ_c, and diffusion mobility, D_c, associated with primary collisions and damage cascade formation. This gives

$$D_F = (\tau_c b_f) \times D_c \qquad (1)$$

And taking that "sphere" of displacements defines characteristic diameter, d, of collision cascade

$$6\tau_c D_c = \frac{d^2}{4} \tag{2}$$

this coefficient can be re-written in a form as follows:

$$D_F = \frac{d^2}{24} b_f \tag{3}$$

Where the rate of generation of damage cascades is

$$b_f = \frac{\pi}{4}(2b)^2 N_s \sigma_{s,n} L_f \varphi \tag{4}$$

Where

$N_s \sigma_{s,n} \varphi$ is the collision rate density, $cm^{-3}s^{-1}$;

$(2b)$ is characteristic diameter of primary collision;

b is the magnitude of the Burgers vector;

$N_s = \omega^{-1}$ is the number density of atoms;

ω is the atomic volume;

$\sigma_{s,n}$ is the average fast neutron scattering cross-section;

L_f is the average length of the damage cascade extension in a polycrystalline material;

φ is the fast neutron flux.

Thus, the following form for the athermal coefficient is obtained:

$$\begin{aligned} D_F &= A_F \varphi \\ A_F &= \frac{\pi}{24} d^2 b^2 N_s \sigma_{s,n} L_f \end{aligned} \tag{5}$$

Substituting into Eq.(5) the values of the constituent parameters according to F.A.Nichols [30] and C.C.Dollins [37] for Zircaloy, the coefficient A_F is obtained as

$$A_F = 2.5 \times 10^{-32}\ cm^4 \tag{6}$$

and the value of the partial self-diffusion coefficient driven by the primary collisions can be simply calculated as

$$D_F = D_{F,ref} \times \frac{\varphi}{\varphi_{ref}} \tag{7}$$

where the normalising reference parameters are chosen as follows:

$$\begin{aligned} D_{F,ref} &= 2.0 \times 10^{-18} cm^2 \times s^{-1} \\ \varphi_{ref} &= 1.2 \times 10^{+14} cm^{-2} \times s^{-1} \end{aligned} \tag{8}$$

Recombination of vacancies and interstitial atoms then occurs after the primary collisions and formation of the damage cascade and the partial interstitial self-diffusion coefficient attributed to this stage is defined here in a form

$$D_R = (b_f \tau_R) \times D_{2,i} \tag{9}$$

where τ_R is the time scale of the quenching phase; $b_f \tau_R$ is the relative time during which diffusion mobility of collided atoms are characterized by $D_{2,i}$, i.e. the interstitial self-diffusion coefficient during the quenching phase.

The time scale in eqn.(9) can be found from the equation of vacancies and interstitial recombination assuming that it can be treated as a stochastic process formalized by Chandrosekhar in ref.[39]. The probability of recombination is proportional to the partial concentrations of defects (interstitial atoms and vacancies), which are virtually equal during the fast quenching phase, their summary diffusion mobility, and effective radius of point defects. If C_R concentration of radiation defects normalized to the number of sites $N_s = \omega^{-1}$ in the elementary volume ω, then equation of stochastic recombination of primary point defects can be written in the form:

$$\frac{d}{d\tau} C_R = -\frac{4\pi b \left(D_{2,v} + D_{2,i}\right)}{\omega} C_R^2, \tag{10}$$

where $D_{2,v}$ is the vacancy self-diffusion coefficient associated with the quenching phase. The quenching stage of cascade damage life can last throughout the time scale τ_R defined from eqn (10), i.e.:

$$\tau_R = \frac{\omega}{4\pi b C_{0,R}} \times \frac{1}{D_{2,v} + D_{2,i}} \tag{11}$$

where $C_{0,R}$ is the equilibrium concentration of point defects at the end of quenching. This concentration from the balance of generation rate and recombination obviously is

$$C_{0R} = \sqrt{\frac{\varphi \sigma_{s,n} L_f}{4\pi b^2} \times \frac{\omega}{D_{2,v} + D_{2,i}}} \tag{12}$$

or

$$C_{0R} = \sqrt{\frac{6\omega^2}{\pi^2 d^2 b^4} \times \frac{D_F}{D_{2,v} + D_{2,i}}} \tag{12'}$$

Substituting parameters expressed by eqns (11) and (12) into eqn (9) gives for the partial irradiation-enhanced self-diffusion coefficient an analytical form as follows:

$$D_R \propto \sqrt{\varphi \times \left(D_{2,v} + D_{2,i}\right)} \tag{13}$$

Taking into account that the diffusion mobility of vacancies in the polycrystalline materials of interest is considerably lower then the mobility of interstitial atoms, then relation (13) is simply

$$D_R \propto \sqrt{\varphi \times D_{2,i}} \tag{13'}$$

and it leads to the normalised representation of the partial coefficient of self-diffusion caused by quenching phase of colliding cascade evolution in the form as follows:

$$D_R = D_{0,R} \sqrt{\frac{\varphi}{\varphi_{ref}}} Exp\left\{-\frac{\Delta E_{m,i}}{2kT}\right\}, \tag{14}$$

where $\Delta E_{m,i} = 0.3\,eV$ is the enthalpy of migration for interstitial atoms in Zircaloy [37] and $D_{0,R}$ is the pre-exponential factor that has can be obtained as best estimation parameter based on data on irradiation-induced self-diffusion. Theoretical value of this factor is of about $1.2 \times 10^{-17}\ cm^2 \times s^{-1}$ [33].

Assuming that the interstitial self-diffusion mechanism dominates at the lattice sites, which belong to the outer zone of the cascade damage, and that the vacancy self-diffusion mechanism acts at the depleted zone, then classic diffusion theory leads to

$$D_T = \sum_{k=1,2} D_{T,k} \sqrt{\frac{\varphi}{\varphi_{ref}}} \times Exp\left\{-\frac{\Delta E_{T,k}}{kT}\right\}, \tag{15}$$

where D_T is the summary self-diffusion coefficient conditioned by migration mechanisms acting at stage of collision cascade annealing; and other parameters are:

$$\Delta E_{T,1} = \Delta E_{m,v} + \Delta E_{f,v} - \frac{1}{2}\Delta E_{m,i} - \delta E \tag{16}$$

$$\Delta E_{T,2} = \frac{1}{2}\Delta E_{m,i} + \delta E \tag{17}$$

and

$\Delta E_{m,i}$ is the interstitial migration enthalpy;

$\Delta E_{m,v}$ is the vacancy migration enthalpy;

$\Delta E_{f,v}$, is the vacancy formation enthalpy.

The parameter δE is the stored energy associated with stresses caused by separation of interstitial atoms into a shell around a vacancy rich internal region of the cascade damage at the late stage of its life. The vacancy in a metallic lattice is a simpler defect and reflects the symmetry of the lattice and also produces considerable relaxation in the elementary lattice cell. In principal, this relaxation can be estimated from the symmetry of arrangement of the sites in the lattice, but anyway it should not exceed the value of the migration enthalpy for the vacancy. In case of Zircaloy type metallic structures the maximum volume relaxation should not exceed ~ 0.25 %, i.e. estimation $\delta E = \Delta E_{f,v} \times 0.75$ is just reasonable.

Pre-exponential factors $D_{T,1}$ *and* $D_{T,2}$ can be confidentially obtained only from analysis of experimental data on thermal annealing of collision cascades. Unfortunately, database available in open literature is not sufficient for model analysis and it necessitates using theoretical estimations for irradiation-enhanced self-diffusion coefficients. For Zircaloy-type materials theory gives (derivation is omitted):

$$D_T = 2.25\times10^{-7} \times \sqrt{\frac{\varphi}{\varphi_{ref}}} \times Exp\left\{-\frac{15668K}{T}\right\}, cm^2 s^{-1} \tag{18}$$

where the interstitial migration mechanism is dominating.

3.7 Polycrystalline Flow Properties

It is well known that the nature of the creep process in a polycrystalline material has either a threshold or non-threshold character or both. However, if plastic deformations generated by dislocation movements in the material are absent due to insufficient intensity of applied stress, then the creep process occurs via self-conjoint mechanisms. That means no voids or break of integrity are associated with the creep, and any single element of structure characterizing diffusion zones of a polycrystalline material, deforms in the group of the other similar structure elements neighboring it. Hence, vacancy flows allowing non-plastic creep deformations are limited inside that structure elements (diffusion zones) and evolution of form of any of those elements processes without changes in volume.

The most energetically favourable reaction at the site of the damage cascade formation is a collapse of vacancy clusters to generate the dislocations, which will act as sinks for interstitial atoms. These dislocations randomly distributed in the polycrystalline material create *de facto* a set of within-grain elements of structure driving their non-plastic and self-conjoint creep deformations. In other words, the macro process of non-threshold thermal creep is allowed due to local vacancy and interstitial flows inside obviously very fine structure elements, which more correctly might be called *diffusion zones*. The essential point is that any macro flow is also arrested.

In polycrystalline materials with anisotropy crystal structures the interaction between neighboring diffusion zones, which is in fact a complicated problem, involving the texture, growth, thermal creep and plastic flows can be easily resolved in terms of viscosity coefficients. External applied stress produces an opposing stress inside of any particular diffusion zone, initiating local vacancy concentration flow between sinks in order to provide relaxation of the applied stress. Representation of polycrystalline materials as an interactive assemblage of single diffusion zones allows defective polycrystalline material to be treated as a viscous compound interpreted in terms of Newtonian and Bingham solid states.

Newtonian viscosity only depends on the effective self-diffusion coefficient of the polycrystalline material and a characteristic distance between the strongest sinks, which in this case coincides with the characteristic size of the diffusion zones in the assemblage. From this point Newtonian viscosity directly is time independent and, thus, a Newtonian viscous compound represents a steady-state component of non-plastic creep and should be associated with mass flow attributed to the vacancy system in the diffusion zones.

If the applied external stress is high enough the Newtonian viscous mass flow cannot provide relaxation of the excess free energy attributed to the stresses in the diffusion zone and dislocation climb will be initiated in order to cope with the stress. Dislocation network defining the diffusion zones should also act as a source of new dislocation loops emitted during movement of the lead dislocation. The viscosity associated with the mass flow in the diffusion zone with dislocations should be considered as the Bingham viscosity.

The Bingham viscosity is more "collective" and has to reflect self-conjoint deformations of the diffusion zones in the highly defective polycrystalline structures under condition of conservation of their volumes. The more accumulated creep deformation, the more relaxation achieved and the less efficient the role of mass flow via the dislocation sub-system. Thus, the treatment of non plastic deformations under applied external stress in terms of the viscous mass flow leads to a representation of the creep process as relaxation from the Bingham to the Newtonian state in the polycrystalline materials.

The introduced approach can be titled as the **BNR** model: **B**ingham-to-**N**ewtonian **R**elaxation creep model.

3.8 BNR Creep Model Equations

The traditional two component creep rate

$$\frac{d\varepsilon_c}{d\tau} = \frac{d\varepsilon_{st}}{d\tau} + \frac{d\varepsilon_{tr}}{d\tau}, \tag{19}$$

where steady-state, *"st"*, and transient, *"tr"*, terms caused by the mass flow via the vacancy and dislocation sub-systems in the diffusion zones correspondingly. Assuming that the strain rate is a sum of Newtonian creep rate and the strain rate produced when a density ρ_n of mobile dislocations is moving at mean group velocity V_n, then the latter can be expressed by E. Orowans's low (in [40], p. 45) and it gives:

$$\frac{d\varepsilon_c}{d\tau} = (\dot{\varepsilon})_{Newtonian} + b\rho_n V_n(S) \tag{20}$$

where S is the applied stress; η_N is the Newtonian viscosity; b is the magnitude of the Burger's vector; ρ_n is the dislocation density associated with the characteristic dimension of diffusion zones (hereafter, such dislocations are called network dislocations and ρ_n is their density). The group velocity V_n of moving dislocations in terms of viscous-diffusion theory can be expressed by general equation as follows:

$$V_n = \frac{D_{Bing}}{kT} \times \frac{\delta W}{\delta L} \tag{21}$$

where D_{Bing} is the effective self-diffusion coefficient to be associated with dislocation mobility due to matterial flow in the diffusion zones; δW is the energy needed to support the dislocation movement over the distance of δL under applied external stress. The characteristic distance due to Orowan's low is simply related with creep:

$$\delta L = \frac{\varepsilon_c + \varepsilon_f}{\rho_n b} \tag{22}$$

where ε_f is the deformation of diffusion zones caused by network dislocations:

$$\varepsilon_f = \pi b^2 \rho_n \tag{23}$$

The elastic energy, ωS, needed to initiate and support the dislocation climbing is increased by factor n due to the elastic stresses from the side of a group of n arrested dislocations related to the lead moving dislocation, i.e., $\delta W = \omega n S$.

Elementary dislocation theory (e.g. [41,42]) allows the n-number to be found as a function of elastic properties of the diffusion zone: $(n)_{Cottrell} = 2S/S_0'$ [43], if stresses S not too much differ from S_0' where

$$S_0' = S_0 Exp\left\{\frac{\omega S_0}{kT} Ln\left(b\sqrt{\pi\rho_n}\right)\right\} \tag{24}$$

$$S_0 = \frac{\mu b\sqrt{\pi\rho_n}}{2\pi(1-\nu)}, \tag{24'}$$

and μ - is the shear modulus; ν - is the Poisson's ratio, and S_0 is the stress, which any particular dislocation experiences as a result of the forces exerted on it by its neighbors, when the distribution of dislocation position and sign in a lattice is random [40]. Exponential factor is due to correction to account stress-induced emission of point defects in diffusion zone.

At stresses $S >> S_0'$ and high temperatures combined effect of temperature and stress lead to increase a number of dislocation loops in pile. The term "high" for temperature means the values when vacance self-diffusion starts to dominanate over interstitial mechanism of self-diffusion.

The Cottrell's number of dislocations participating to Bingham diffusion creep is to be increased from first power to power between 2 to 3. From general consideration the total number as a function of stress and temperature can be postulated in a form as follows:

$$n = 2\times\left(S/S_0'\right)^{1+\Delta\alpha(S,T)} \tag{25}$$

$$\Delta\alpha = \Delta\alpha_0 \times\left(1-Exp\left\{-\frac{S-S_0'}{S_0'}\right\}\right)\times\left(1-\left\{-\frac{T-T_\rho}{\Delta T_\rho}\right\}\right) \tag{25'}$$

The definition of empirical parameters $\Delta\alpha_0, T_\rho, \Delta T_\rho$ will be discussed below.

The vacancy diffusion creep rate in terms of the Newtonian viscosity should be defined via characteristic size of diffusion zones [40], i.e.:

$$(\dot{\varepsilon})_{Newtonian} = \frac{S}{\eta_N}; where\ \eta_N = \frac{kT\, g_{eqv}^2}{4\omega D_{eff}} \tag{26}$$

where D_{eff} - is the effective volume self-diffusion coefficient; g_{eqv} is the equivalent (characteristic) size of diffusion zones evaluated above. This size is not the same as grain size. Network dislocations, which may act as vacancy sources and sinks, create some kind of sub-grains within course grain structure of polycrystalline material. Where climbing dislocations are the sources and sinks, characteristic parameter of Newtonian viscosity becomes the average size of pseudo sub-grain structure (and real sub-grain structure as well) [40]. Lifshitz [44] long ago recognized that, in a polycrystal, if grains were deformed by diffusion creep, then grain-boundary sliding would have to take place, otherwise holes would form at the boundaries on which the vacancies were depositing. Herring [45] had pointed out earlier that the diffusion strain rate calculated for a single crystal must be quite close to that of a polycrystal, because although local stresses are set up as a grain-packing adjusts to prevent hole-formation, these stresses should be rapidly smoothed out by the diffusion process. When, under stresses, the individual grains have undergone diffusion creep, the vacancies that have precipitated tend to form voids, unless sliding occurs simultaneously to prevent void-formation. It was shown in analysis by Cannon [46].

At the grain boundaries, where climbing dislocations are the sources and sinks, the characteristic size of diffusion zone becomes average distance between dislocations (i.e. $1/\sqrt{\rho_n}$) [40] and, hence, grain deformation due to diffusion creep is simply $\pi G^2/\sqrt{\rho_n}$. It means, at the same time, that diffusion zones in grain volume must adjust such deformation simultaneously to prevent holes- formation in grain volume. This enables evaluation for the characteristic size of the diffusion zones in grain volume as follows: $\frac{\pi}{6} g_{eqv}^3 = \pi G^2/\sqrt{\rho_n}$ or:

$$g_{eqv} = G \times \left(\frac{6}{\sqrt{\rho_n G^2}} \right)^{\frac{1}{3}} \tag{27}$$

The dynamic of the diffusion creep process due to Newtonian and Bingham vicious flow after all can be given by the equation as follows:

$$\frac{d\varepsilon_c}{d\tau} = A + \frac{B}{\varepsilon_c + \varepsilon_f} \tag{28}$$

where

$$A = 4 \times g_{eqv}^{-2} D_{eff} \frac{\omega S_0'}{kT} \times \left(\frac{S}{S_0'} \right) \tag{29}$$

$$B = \rho_n D_{Bing} \times \frac{\omega S_0'}{kT} \times \frac{2}{\pi} \times \varepsilon_f \times \left(\frac{S}{S_0'} \right)^{2+\Delta\alpha(S,T)} \tag{30}$$

Bingham function parameter expressed by eq.(30) can be re-written via *Sinh* that is more adequate form [40] and more convenient for any practical calculations. This form is given by

$$B = \frac{2}{\pi} \times \rho_n D_{Bing} \times \frac{\omega S_0'}{kT} \varepsilon_f \times \left(Sinh \frac{S}{S_0'} \right)^{2+\Delta\alpha(S,T)}$$

The closed form solution of eq. (28) is

$$\varepsilon_c = \varepsilon_0 + A\Delta\tau + \frac{B}{A} Ln \left\{ \frac{\varepsilon_c + \varepsilon_f + \frac{B}{A}}{\varepsilon_0 + \varepsilon_f + \frac{B}{A}} \right\} \tag{31}$$

where $\Delta\tau = \tau - \tau_0$ and $\varepsilon_0 = \varepsilon(\tau_0)$. The approximate solution for the creep equation can be presented simply as:

$$\varepsilon = A\Delta\tau + \sqrt{(\varepsilon_0 + \varepsilon_f)^2 + 2B\Delta\tau} - \varepsilon_f \tag{32}$$

Two function parameters of the **BNR**-creep model are of considerable importance in controlling a wide range of physical and mechanical properties of polycrystalline materials under irradiation and out-of-reactor conditions. These are the effective self-diffusion coefficient and the density of network dislocations. There are two types of defects in polycrystalline materials, which have to be considered in the context of the diffusion problem, the vacancy dislocation loops, which are the most favourable energetically and have to be formed as a result of collision cascades collapse, and network dislocations. Once created, any particular depleted zone of the collapsed cascade is a sink for the point defects created at other cascade zones. Since interstitial atoms migrate more rapidly than vacancies in the metals of interest, most of the point defects, which escape cascade zones are interstitial atoms and most of the point defects that arrive at the zone are interstitial atoms as well. This results in healing of the collapsed cascade zone.

The process should look like the recombination of interstitial atoms arriving at a depleted zone with vacancy loops formed at the site of the collapsed cascade.

The rate of recombination depends on three factors. These are (a) the mobility of interstitial atoms arriving from other zones directly at the site of vacancy loop and characterised by the self-diffusion coefficient $D_{T,2}$, (b) the rate at which the vacancies of the depleted zone can migrate in their spongy configuration in the depleted zone with self-diffusion coefficient $D_{T,1}$ and (c) the volume density of the vacancy loops.

The vacancy dislocation loops as recombination centres trap interstitial atoms and effectively reduce their acting mobility. If N_L is the number of such loops per unit volume and R_L is the effective radius characterising the recombination centre formed by cascade collapse, then the probability per unit time for interstitial atoms to be trapped by such a recombination centre is simply:

$$a_L = 2\pi R_L N_L D_T \qquad (33)$$

where partial self-diffusion coefficient, D_T, is given by eq.(14). Parameter N_L can be obtained from the value of loop-loop separation distance at the site of cascade collapse. W.J.Phythian has reported [38] that the loop-loop separation distance based on the calculated production data is to be ~ 6 nm in the materials of interest. Taking for the damage cascade diameter a value of ~ 10 nm as it has been obtained experimentally [37], then the volume density of the recombination centres on the sites of collapsed cascades will be ~ $2 \cdot 10^{18}$ cm^{-3}. The characteristic radius of these recombination centres is to be consistent with the radius of the depleted zone of collapsed cascades, which is ~ 1.5-2 nm according to C.C.Dollins [37]. These parameters are used in ***BNR*** creep model equations.

De-trapping is a possible process as a result of thermal emission, which is energetically unfavourable or knocking out from the side of a newly formed damage cascade. This effect knocking out ((de-trapping)) is to be controlled by the rate factor b_f defined by eqn. (4).

If the partial self-diffusion coefficients are known, then a resulting effective coefficient controlling self-diffusion in a polycrystalline mate under fast neutron flux irradiation is:

$$D_{eff} = D_{v,eff} + 2b^2 \rho_n \times D_N , \qquad (34)$$

where

$$D_{v,eff} = D_F + D_R + D_T \times \frac{b_f}{b_f + a_L} \tag{35}$$

for a polycrystalline under irradiation conditions, or

$$D_{v,eff} = D_{th}(T) \tag{35`}$$

without irradiation, where D_{th} is the thermal self-diffusion coefficient for unirradiated polycrystalline material, and

$$D_{Bing} = \pi b^2 \rho_n \times D_N \times \frac{a_L}{b_f + a_L} + D_T \times \frac{b_f}{b_f + a_L} \tag{36}$$

where D_N is the self-diffusion coefficient associated with the interstitial mobility at the dislocation sites:

$$D_N = D_{0,N} \times Exp\left\{-\frac{Q_N + \Delta Q_{el}}{kT}\right\} \tag{37}$$

and parameter ΔQ_{el} reflects the elastic influence on the equilibrium concentration of point defects at a site of network dislocation from the neighbouring dislocations:

$$\Delta Q_{el} = \frac{\mu\omega b\sqrt{\pi\rho_n}}{2\pi(1-\nu)} Ln\left(b\sqrt{\pi\rho_n}\right) \tag{38}$$

As-fabricated polycrystalline material contains a stress independent density of network dislocations formed during the manufacturing process. For unirradiated Zircaloy-4 the initial network dislocation density, $\rho_{0,n}$, is rather high, i.e. ~10^{10} to 10^{11} cm^{-2} [47]. Under irradiation with fast neutron flux an initial network dislocation density comes under the influence of resolution effects from the side of continuously formed cascades, due to that it is gradually "melted" and, hence, tends to some equilibrium limit.

The equilibrium density of network dislocations controlling the viscous flow properties and the characteristic size of diffusion zones under fast neutron irradiation can be estimated by assuming that one diffusion zone is formed per each high energy primary knock-on. It gives:

$$\rho_{n,irr} \cong \frac{1}{d^2}\left\{\frac{2}{\pi}\frac{d}{L_f}\right\}^{\frac{2}{3}} = 8 \times 10^9 cm^{-2} \tag{39}$$

and the density of the diffusion zones, ρ_n, for any particular time period can then be presented in a form as:

$$\rho_n(\tau) = \rho_{n,irr} + \left(\rho_n(\tau_o) - \rho_{n,irr}\right) Exp\left\{-\frac{\Delta\tau \times \varphi}{F_s}\right\} \qquad (40)$$

where F_s is the material dependent parameter with the dimension of fluence and characterising the rate of relaxation of density of the diffusion zones under fast neutron flux, φ, irradiation. The values 10^{20} and 10^{21} n/cm^2 for F_s parameter for Zr+1%Nb and Zircaloy-4 are correspondingly applied in the ***BNR*** creep model.

The values for $D_{0,N}$ and Q_N can be calculated theoretically, but currently they are "free" parameters of the BNR-model and are obtained from model interpretation of out-of-pile thermal creep data [48,49]. A few examples of the ***BNR***-creep model calculations for one set of parameters as for Zircaloy-4 are illustrated at Figures 1 and 2 in comparison with out-of-pile experimental data available due to [48,49]. The temperatures were not high to initiate emission of stress-temperature induced dislocation loops and parameter $\Delta\alpha(S,T) \approx 0$. So these two examples demonstrate principal applicability of "theoretical" part of the ***BNR***-creep equation expressed by (28) along with function parameters (29) and (30). For the non-linear stress-temperature function $\Delta\alpha(S,T)$ introduced empirically by form (26), the values of parameters $\Delta\alpha_0, T_\rho, \Delta T_\rho$ were derived based on comparison between model calculations and creep data for high temperature (675 K) as available due to reference [48]. The set of parameters $\Delta\alpha_0 = 1.5$, $T_\rho = 615\,K$, $\Delta T\rho = 25\,K$ has been obtained to simulate very closely experimental data as shown in Figure 3. After calculations the values for $D_{0,N}$ and Q_N as follows: $D_{0,N} = 1.5 \times 10^8\ cm^2 s^{-1}$ and $Q_N = 269\,kJ/mol$ as the best fit to the experimental data have been derived.

Figures 4 and 5 show the typical results of BNR-creep model predictions for commercial PWR fuel rods and one test fuel rod. These results are only qualitative and are to demonstrate good consistence with PIE data reported for instance in [49,50].

3.9 Synopsis and Conclusions

A new diffusion creep model for polycrystalline materials such as Zircaloy-4 has been developed and proposed. The model entitled ***BNR***-creep model - **B**ingham-to-**N**ewtonian **R**elaxation of diffusion zones - was constructed under ambitions "*from first principles - to principal practice applications*". The complexity of the ***BNR***-creep model suits the level needed for calculation with fuel performance computer codes.

Thermal creep in polycrystalline alloys differs significantly from that under neutron irradiation at the same temperature level. Under neutron irradiation, for instance, model calculations predict a creep down of the LWR fuel rod cladding at a relatively high rate at the beginning-of-life if a neutron fluence is below ~ 10^{20}-10^{21} n/cm^2 and a considerably slow down when fluence is proceeding to increase. In out-of-pile thermal creep tests the process develops more gradually. But the nature of the process in both cases is the same and can be satisfactorily explained in terms of viscous Newtonian and Bingham flow properties mainly controlled by self-diffusion of the point defects in polycrystalline and network dislocations.

It is network dislocation density evolution with neutron irradiation that most likely responsible for the observed differences in the thermal creep under irradiation and out-of-pile tests at reference temperatures and stresses.

In terms of the formulated viscous approach an increase in the yield strength with fluence to some upper limit at fixed temperatures simply reflects evolution of the network dislocations with fast neutron fluence and an increasing of the characteristic size of the diffusion zones.

Neutron irradiation becomes a key factor of thermal creep due to mainly two effects: irradiation-induced and irradiation-enhanced self-diffusion mechanisms and lattice microstructure changes driving restructuring of an initial network of dislocations and falling of their density to an equilibrium limit. The limit itself (after relatively short radiation time) is controlled by the characteristic size of damage cascades initiated by fast neutron knock-on effects. From a methodological position, the Newtonian and Bingham viscous mechanisms of flow in polycrystalline materials being re-formulated in terms of diffusion zones capable to explain the macro-process (thermal creep) via very localized mass flows. And no macro mass transfer is needed to support the thermal creep process in polycrystalline materials such as Zircaloy-4.

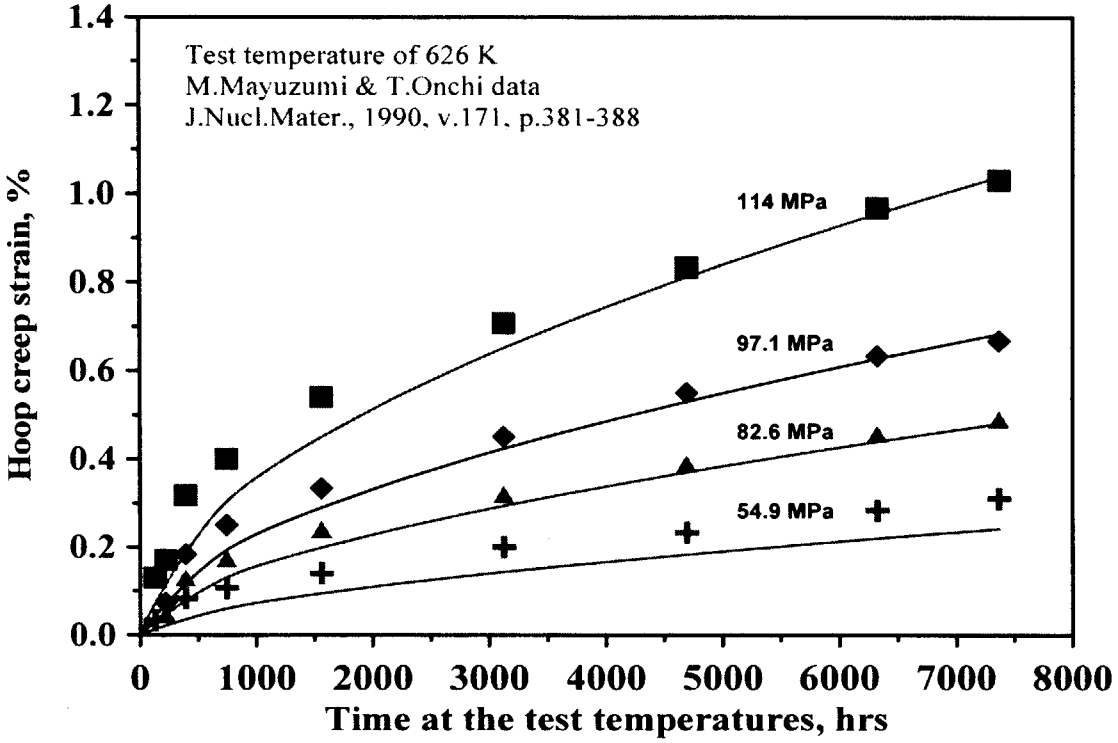

Hoop creep strain in Zircaloy-4 fuel rod cladding as measured and calculated with BNR-creep model

Figure 1.

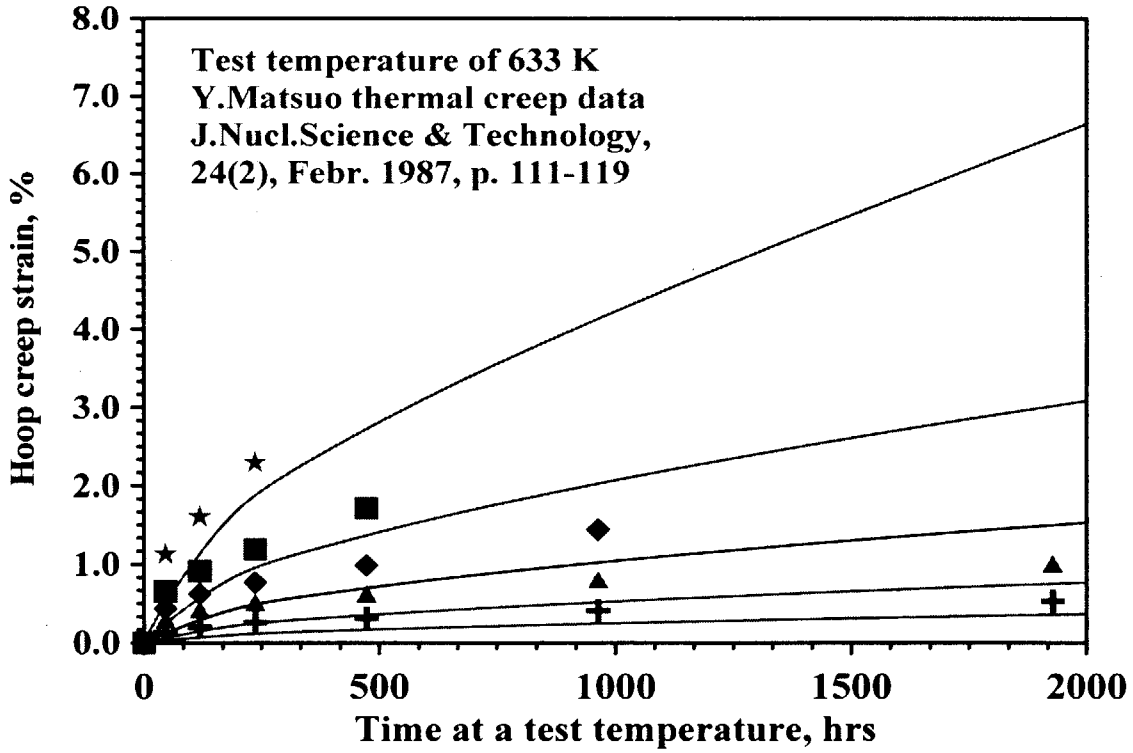

Hoop creep strain in Zircaloy-4 fuel rod cladding as measured and calculated with BNR-creep model

Figure 2.

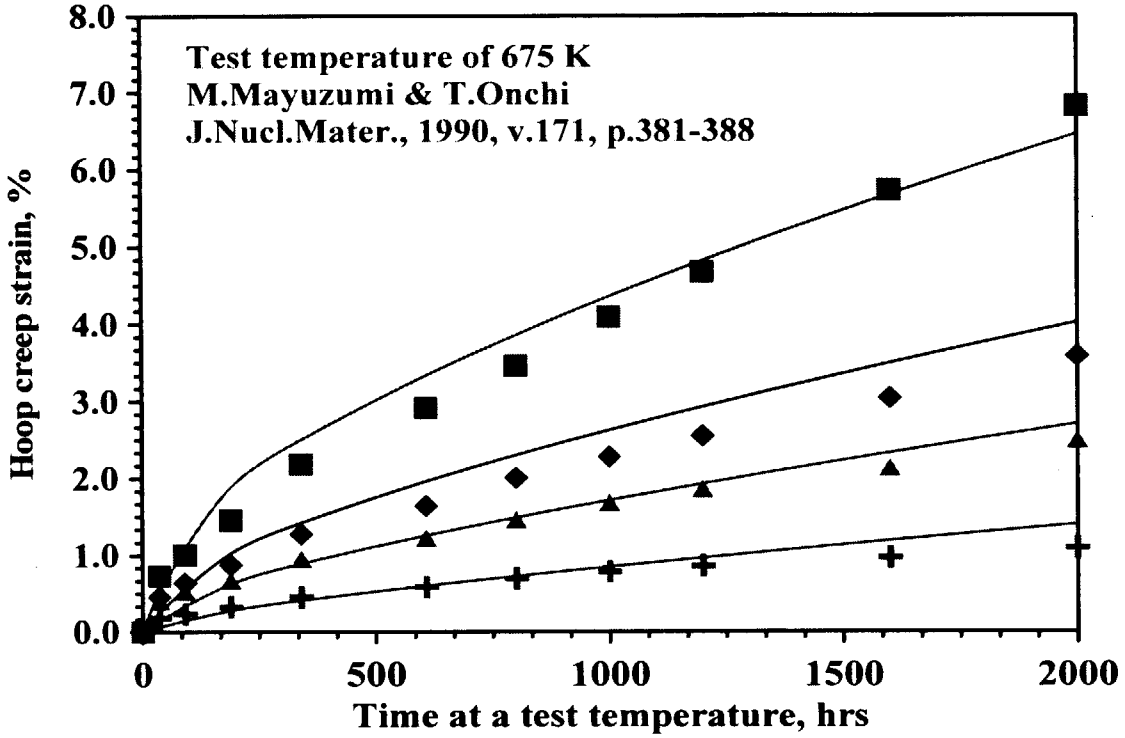

Hoop creep strain in Zircaloy-4 fuel rod cladding as measured and calculated with BNR-creep model

Figure 3.

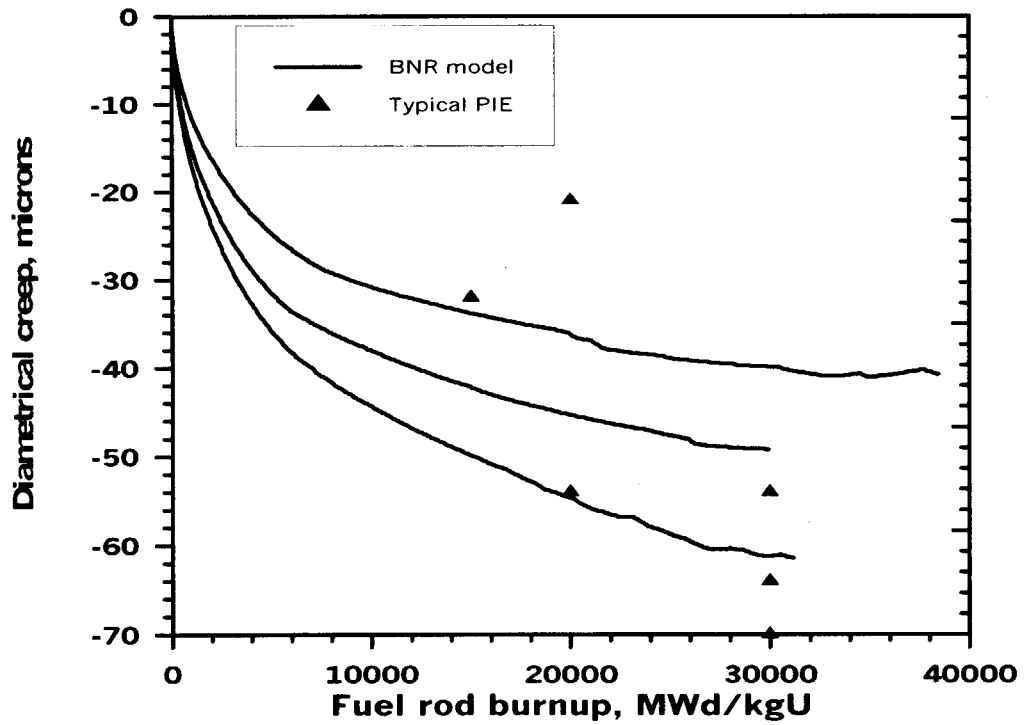

Figure 4. Qalitative comparison of BNR-creep model predictions for PWR type fuel rods verses typical PIE data as reported by W.E. Baily et al. [13])

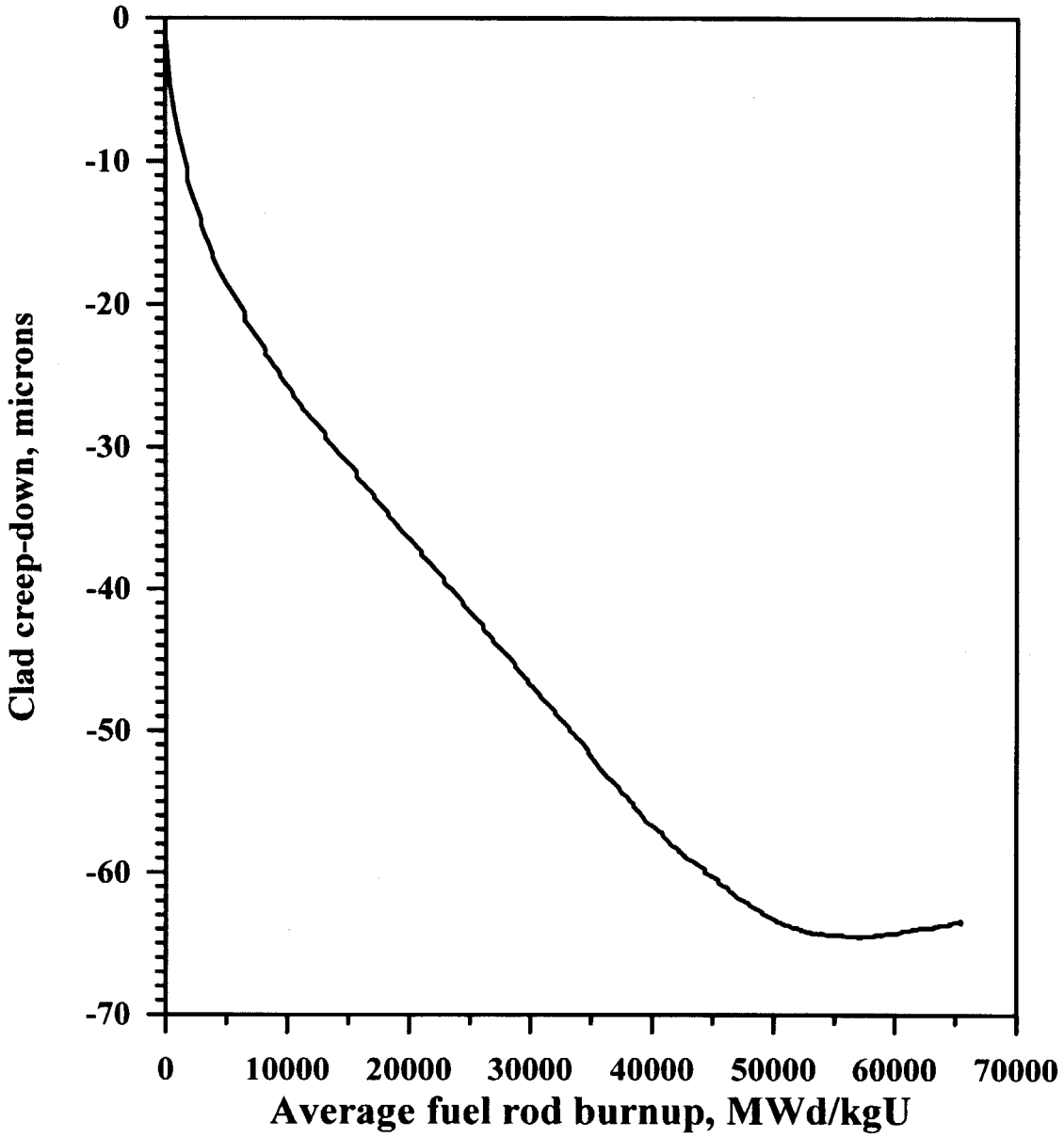

Figure 5. Illustrative calculations of clad creep-down for the test fuel rod BK-356

(PIE data showed creep down in active clad length from 51 to 72 μm [51])

REFERENCES

1. C. T. Walker and M. Coquerelle, Correlation between Microstructure and Fission Gas Release in High Burnup Fuels, ANS International Topical Meeting on LWR Fuel Performance, Avignon, France, April 21-24, 1991.
2. R. Manzel and R. Eberly, Fission Gas Release at High Burnup and the Influence of the Pellet Rim, ibid.
3. J. O. Barner, M. E. Cunningham, M. D. Freshley, D. D. Lunning, Relationship between Microstructure and Fission Gas Release in High Burnup UO_2 Fuel With Emphasis on the Rim Region, ibid.
4. K. Lassmann, C. T. Walker, J. van de Laar, F. Lindström, Modelling the High Burnup UO2 Structure in LWR Fuel, J. Nucl. Mater., 226 (1995) p. 1-8
5. K. Lassmann, C. O'Carroll, J. van de Laar and C. T. Walker, The Radial Distribution of Plutonium in High Burnup UO_2 fuels. J. Nucl. Mater. 208 (1994) p. 223-231.
6. T. Nakajima, H. Saito, and T. Osaka, FEMAXI-IV: A Computer Code for the Analysis of Thermal and Mechanical Behavior of Light Water Reactor Fuel Rods. Nucl. Eng. Design 148, 1994, p. 41-52
7. M. Suzuki and H. Saito, Light Water Reactor Fuel Analysis Code FEMAXI-IV Version 2, JAERI-DATA/CODE, 97-043, 1997.
8. M. E. Cunningham, D. D. Lanning, J. O. Barner, Qualification of Fission Gas Release Data from Task 3 rods. HBEP-60 (3P26), Battelle Pacific Northwest Laboratories, Richland, WA, January 1990.
9. R. M. Cornell, An Electron Microscope Examination of Matrix Fission-gas Bubbles in Irradiated Uranium Dioxide, J. Nucl. Mater. 38 (3), 1971, p. 319-328.
10. J. A. Turnbull, The Distribution of Intragranular Gas Bubbles in UO_2 during Irradiation, J. Nucl. Mater. 38 (2), 1971, p. 203-212
11. C. Baker, The Fission Gas Bubble Distribution in Uranium Dioxide from High Temperature Irradiated SGHWR Fuel Pins, J. Nucl. Mater. 66, 1977, p. 283-291.
12. C. Baker, The Fission Gas Bubbles Distribution in a Mixed Oxide Fast Reactor Fuel Pin, J. Nucl. Mater. 75, 1978, p. 105-109

13. M. O. Marlowe and A. I. Kaznoff, in: Proc. International Conf. Nuclear Fuel Performance (Brit. Nucl. Energy Soc., London, 1973).

14. C. Baker, Central Electricity Generating Board Research Report RD-B-N4194 (1997).

15. M. H. Wood, Modelling Bubble Nucleation and Fission-Induced Re-Solution in Nuclear Fuel, J. Nucl. Mater. 82 (1979) p. 264-270.

16. J. A. Turnbull, C. A. Friskney, et al., The Diffusion Coefficients of Gaseous and Volatile Species during the Irradiation of Uranium Dioxide, J. Nucl. Mater. 107 (1982) 168-184.

17. R. J. White, P. A. Tempest, P. Wood, An Evaluation of Diffusion Coefficient Data Obtained from Start-up RAMP of IFA-563 and Comparison with Data from the Gas Flow Rigs IFA-504 and IFA-558. – HPR-343/23, 1993

18. S. E. Lemekhov, Towards Mechanistic Understanding of FGR and Related Processes at Extended Burnup, ANS Topical Meeting on Light Water Reactor Fuel Performance, West Palm Beach, 17-21 April, 1994.

19. J. A. Turnbull, A Review of the Thermal Behaviour of Nuclear Fuel, Thermal Performance of High Burn-up LWR Fuel, Seminar Proceedings, Cadarache, France, 3-6 March 1998.

20. S. E. Lemekhov, H. Devold, Model Analysis of the HBWR IFA-503.1 PWR/WWER Comparative Test Results, HWR-482, 1996.

21. M. Uchida and H. Saito, RODBURN: A Code for Calculating Power Distribution in Fuel Rods. JAERI-M 93-108, 1993.

22. D. D. Lanning, C. E. Beyer, C. L. Painter, FRAPCON-3: Modifications to Fuel Rod Material Properties and Performance Models for High-Burnup Application. NUREG/CR-6534, Volume 1, PNNL-11513, 1997.

23. S. E. Lemekhov, ASFAD Code Calculations for WWER-440 High Burnup Fuel Rods, Second International Seminar on WWER Fuel Performance, Modelling and Experimental Support, Sandanski, Bulgaria, 21025 April, 1997.

24. I. D. Palmer, K. W. Hesketh and P.A. Jackson, Water Reactor Fuel Element Performance Computer Modelling, ed. J. Gittus (Applied Science, Barking, UK, 1983) p. 321.

25. S. E. Lemekhov, Thermodynamic of the High Burnup UO_2 Structure Formation and Fission Gas Release, ANS Topical Meeting on LWR Fuel Performance, March 2-6, 1997, Portland, Oregon.

26. S. E. Lemekhov, H. Devold, V. V. Yakovlev, Comparison of Thermal and Mechanical Behaviour of PWR/WWER fuel in IFA-503, HWR-467, 1996.

27. S. E. Lemekhov, In-Reactor Densification Behaviour of UO_2 LWR Fuel and Modelling, Proceeding of Second Seminar on WWER Fuel Performance, Modelling and Experimental Support, Sandanski, Bulgaria, April 21-25, 1997.

28. M. Oguma, Cracking and Relocation Behaviour of Nuclear Fuel Pellets during Rise to Power, Nuclear Engineering and Design, 76 (1983), p. 35-45.

29. S. E. Lemekhov, An Analytical Method for Investigation of In-Pile Densification of Uranium Dioxide Fuel Pellets Based on Rise to Power Data. Preprint KIAE-5237/11, Kurchatov Institute, Moscow, 1990.

30. F. A. Nichols, Theory of the Creep of Zircaloy during Neutron Irradiation, J. Nucl. Mater. 30 (1969) 249-270

31. J. R. Matthews and M. W. Finnis, Irradiation Creep Models – An Overview, J. Nucl. Mater. 159 (1988) 257-285

32. N. E. Hoppe, Engineering Model for Zircaloy Creep and Growth. ANS Topical Meeting on Light Water Reactor Fuel Performance, Avignon, France, April 21-24, 1991, p. 201-207

33. S. E. Lemekhov, LWR Fuel Rod Clad Creep Behaviour Modelling, Proceeding of Second Seminar on WWER Fuel Performance, Modelling and Experimental Support, Sandanski, Bulgaria, April 21-25, 1997.

34. A. V. Smirnov, V. A. Tsibulya, K. P. Dubrovin, et al., Experimental Support of WWER-440 Fuel Reliability and Serviceability at High Burnup, International Seminar on WWER Fuel Performance, Modelling and Experimental Support, Varna, St. Constantine, 7-11 November, 1994.

35. K. Une, K. Nogita, S. Kashibe, T. Royonaga, and M. Amaya, Effect of Irradiation Induced Microstructural Evolution of High Burnup Fuel Behaviour, ANS Topical Meeting on Light Water Reactor Fuel Performance, Portland, Oregon, March 2-6, 1997, p. 478-489.

36. S. E. Lemekhov, Computer Code ASFAD: Status, Recent Developments and Applications, ANS Topical Meeting on Light Water Reactor Fuel Performance, West Palm Beach, 17-21 April, 1994.

37. C.C.Dollins, "In-pile Temperature Dependence of the Yield Strength and Growth of Zircaloy", J. Nucl. Mater., vol. 82, 1979, p.311-316

38. W.J.Phythian, "Displacement Collision Cascade Damage in HCP Metals", J. Nucl. Mater., vol. 159, 1988, p.219-224.

39. S. Chandrosekhar, Stochastic Problems in Physics and Astronomy. Review of Modern Physics, 15 (1943) 1-89.

40. John Gittus, Creep, Viscoelasticity and Creep Fracture in Solids, Applied Science Publishers Ltd. 1975.

41. J.Weertman, J.R.Weertman, "Elementary Dislocation Theory". London, 1964.

42. F.R.N.Naborro, "Theory of crystal dislocations". Oxford, 1967.

43. A. H. Cottrell, Dislocations and Plastic Flow, Oxford Univ. Press. 1953.

44. I. M. Lifshitz, Soviet Physics, 17, 909, 1963.

45. C. Herring, J. Appl. Phys., 21, 1950, p. 437

46. W. R. Cannon, The Contribution of Grain-Boundary Sliding to Axial Strain during Diffusion Creep, Phil. Mag., 25, 1972, p. 1489-1497.

47. A.V.Nikulina, V.A.Markelov, M.M.Peregud, et al. "Irradiation-Induced Microstructure Changes in Zr-1%Sn-1%Nb-0.4%Fe". - J. Nucl. Mater., vol. 238, 1996, p.205-210.

48. Y.Matsuo, "Thermal Creep of Zircaloy-4 Cladding under Internal Pressure". Journal of Nuclear Science & Technology, 1987, 24(2), p. 111-119.

49. M.Mayuzumi, Takeo Onchi, "Creep Deformation of an Unirradiated Zircaloy Nuclear Fuel Cladding Tube Under Dry Storage Conditions". - Journal of Nuclear Material, vol. 171, 1990, p.381-388.

50. W.E. Baily et al., ANS International Topical Meeting on LWR Fuel Performance, Orlando, Florida, (1985), p. 1.

51. NDT Examinations of Eighteen Fuel Rods Irradiated for Three or Four Cycles in BR-3, HBEP-56 (3P22), June 1989

This is a blank page.

国際単位系（SI）と換算表

表1　SI基本単位および補助単位

量	名称	記号
長さ	メートル	m
質量	キログラム	kg
時間	秒	s
電流	アンペア	A
熱力学温度	ケルビン	K
物質量	モル	mol
光度	カンデラ	cd
平面角	ラジアン	rad
立体角	ステラジアン	sr

表2　SIと併用される単位

名称	記号
分，時，日	min, h, d
度，分，秒	°, ′, ″
リットル	l, L
トン	t
電子ボルト	eV
原子質量単位	u

1 eV=1.60218×10^{-19}J

1 u=1.66054×10^{-27}kg

表5　SI接頭語

倍数	接頭語	記号
10^{18}	エクサ	E
10^{15}	ペタ	P
10^{12}	テラ	T
10^{9}	ギガ	G
10^{6}	メガ	M
10^{3}	キロ	k
10^{2}	ヘクト	h
10^{1}	デカ	da
10^{-1}	デシ	d
10^{-2}	センチ	c
10^{-3}	ミリ	m
10^{-6}	マイクロ	μ
10^{-9}	ナノ	n
10^{-12}	ピコ	p
10^{-15}	フェムト	f
10^{-18}	アト	a

表3　固有の名称をもつSI組立単位

量	名称	記号	他のSI単位による表現
周波数	ヘルツ	Hz	s^{-1}
力	ニュートン	N	m·kg/s^2
圧力，応力	パスカル	Pa	N/m^2
エネルギー,仕事,熱量	ジュール	J	N·m
工率，放射束	ワット	W	J/s
電気量，電荷	クーロン	C	A·s
電位，電圧，起電力	ボルト	V	W/A
静電容量	ファラド	F	C/V
電気抵抗	オーム	Ω	V/A
コンダクタンス	ジーメンス	S	A/V
磁束	ウェーバ	Wb	V·s
磁束密度	テスラ	T	Wb/m^2
インダクタンス	ヘンリー	H	Wb/A
セルシウス温度	セルシウス度	℃	
光束	ルーメン	lm	cd·sr
照度	ルクス	lx	lm/m^2
放射能	ベクレル	Bq	s^{-1}
吸収線量	グレイ	Gy	J/kg
線量等量	シーベルト	Sv	J/kg

表4　SIと共に暫定的に維持される単位

名称	記号
オングストローム	Å
バーン	b
バール	bar
ガル	Gal
キュリー	Ci
レントゲン	R
ラド	rad
レム	rem

1 Å=0.1nm=10^{-10}m

1 b=100fm^2=10^{-28}m^2

1 bar=0.1MPa=10^{5}Pa

1 Gal=1cm/s^2=10^{-2}m/s^2

1 Ci=3.7×10^{10}Bq

1 R=2.58×10^{-4}C/kg

1 rad=1cGy=10^{-2}Gy

1 rem=1cSv=10^{-2}Sv

（注）

1．表1－5は「国際単位系」第5版，国際度量衡局1985年刊行による。ただし，1eVおよび1uの値はCODATAの1986年推奨値によった。

2．表4には海里，ノット，アール，ヘクタールも含まれているが日常の単位なのでここでは省略した。

3．barは，JISでは流体の圧力を表わす場合に限り表2のカテゴリーに分類されている。

4．EC閣僚理事会指令ではbar，barnおよび「血圧の単位」mmHgを表2のカテゴリーに入れている。

換算表

力	N(=10^{5}dyn)	kgf	lbf
	1	0.101972	0.224809
	9.80665	1	2.20462
	4.44822	0.453592	1

粘度　1Pa·s(N·s/m^2)=10P(ポアズ)(g/(cm·s))

動粘度　1m^2/s=10^{4}St(ストークス)(cm^2/s)

圧力	MPa(=10bar)	kgf/cm^2	atm	mmHg(Torr)	lbf/in^2(psi)
	1	10.1972	9.86923	7.50062×10^3	145.038
	0.0980665	1	0.967841	735.559	14.2233
	0.101325	1.03323	1	760	14.6959
	1.33322×10^{-4}	1.35951×10^{-3}	1.31579×10^{-3}	1	1.93368×10^{-2}
	6.89476×10^{-3}	7.03070×10^{-2}	6.80460×10^{-2}	51.7149	1

エネルギー・仕事・熱量	J(=10^7 erg)	kgf·m	kW·h	cal(計量法)	Btu	ft·lbf	eV
	1	0.101972	2.77778×10^{-7}	0.238889	9.47813×10^{-4}	0.737562	6.24150×10^{18}
	9.80665	1	2.72407×10^{-6}	2.34270	9.29487×10^{-3}	7.23301	6.12082×10^{19}
	3.6×10^6	3.67098×10^5	1	8.59999×10^5	3412.13	2.65522×10^6	2.24694×10^{25}
	4.18605	0.426858	1.16279×10^{-6}	1	3.96759×10^{-3}	3.08747	2.61272×10^{19}
	1055.06	107.586	2.93072×10^{-4}	252.042	1	778.172	6.58515×10^{21}
	1.35582	0.138255	3.76616×10^{-7}	0.323890	1.28506×10^{-3}	1	8.46233×10^{18}
	1.60218×10^{-19}	1.63377×10^{-20}	4.45050×10^{-26}	3.82743×10^{-20}	1.51857×10^{-22}	1.18171×10^{-19}	1

1 cal=4.18605J（計量法）

=4.184J（熱化学）

=4.1855J（15℃）

=4.1868J（国際蒸気表）

仕事率　1PS(仏馬力)

=75 kgf·m/s

=735.499W

放射能	Bq	Ci
	1	2.70270×10^{-11}
	3.7×10^{10}	1

吸収線量	Gy	rad
	1	100
	0.01	1

照射線量	C/kg	R
	1	3876
	2.58×10^{-4}	1

線量当量	Sv	rem
	1	100
	0.01	1

（86年12月26日現在）

ON THE DEVELOPMENT OF LWR FUEL ANALYSIS CODE (1) — ANALYSIS OF THE FEMAXI CODE AND PROPOSAL OF A NEW MODEL —